Device optimization of tris-aluminum (Alq_3) based bilayer organic light emitting diode structures

J. Chan,[1] A. D. Rakić,[1*] C. Y. Kwong,[2] Z. T. Liu,[3] A. B. Djurišić[3], M. L. Majewski,[1]

W. K. Chan[4] and P. C. Chui[2]

[1]School of Information Technology and Electrical Engineering, The University of Queensland,

Brisbane Qld4072, Australia

[2]Department of Electrical & Electronic Engineering, University of Hong Kong,

Pokfulam Road, Hong Kong

[3]Department of Physics, University of Hong Kong,

Pokfulam Road, Hong Kong

[4]Department of Chemistry, University of Hong Kong,

Pokfulam Road, Hong Kong

Abstract

In this work we present detailed analysis of the emitted radiation spectrum from tris(8-hydroxyquinoline) aluminum (Alq_3) based bilayer OLEDs as a function of: the choice of cathode, the thickness of organic layers, and the position of the hole transport layer/Alq_3 interface. The calculations fully take into account dispersion in the glass substrate, the indium tin oxide anode, and in the organic layers, as well as the dispersion in the metal cathode. Influence of the incoherent transparent substrate (1 mm glass substrate) is also fully accounted for. Four cathode structures have been considered: Mg/Ag, Ca/Ag, LiF/Al, and Ag. For the hole transport layer, N,N'-diphenyl-N,N'-(3-methylphenyl)-1,1'-biphenyl-4,4'-diamine (TPD) and N,N′-di(naphthalene-1-yl)-N,N′-diphenylbenzidine (NPB) were considered. As expected, emitted radiation is strongly dependent on

the position of the emissive layer inside the cavity and its distance from the metal cathode. Although our optical model for an OLED does not explicitly include exciton quenching in vicinity of the metal cathode, designs placing the emissive layer near the cathode are excluded to avoid unrealistic results. Guidelines for designing devices with optimum emission efficiency are presented. Finally, several different devices were fabricated and characterized and experimental and calculated emission spectra were compared.

Keywords: organic light emitting diodes, device design

* Email : rakic@itee.uq.edu.au

1. INTRODUCTION

Organic light emitting diodes (OLEDs) are attracting increasing attention for applications in display devices due to their high brightness and wide viewing angle [1-2]. While there has been significant progress in this area over recent years, comprehensive optical studies on device simulation and design have been scarce. The simulations of the charge transport and charge distribution in organic light emitting devices have been reported [3-4]. There have been several works on calculating the emission pattern [5] and external coupling in OLEDs [6]. It has been shown that the emission from an OLED can be varied through interference effects by changing the thickness of the organic layer in an OLED with a dielectric layer located below the ITO anode [7] or by changing the thickness of a ZnSe layer on top of the metal cathode [8-9]. For an OLED with SiO_2 layer below the ITO, it was shown that the emission spectrum from an OLED is strongly dependent on the Alq_3 thickness, so that with the increase of Alq_3 thickness the emission peak shifts from ~525 nm to ~555 nm, and with further increase of the thickness even splits into two peaks, one located ~495 nm and the other ~590-600 nm [7]. It was also shown that, by changing the thickness of ZnSe layer deposited on top of the cathode, the efficiency of the OLED can be optimized so that for optimal ZnSe thickness efficiency as high as 64 cd/A can be achieved [8-9].

The spectral and angular distribution of the emission from an OLED has been studied in more detail in organic microcavity devices [10-11] than in non-cavity devices. However, if we consider a typical OLED structure consisting of a glass substrate, ITO anode, hole transport layer (HTL), emitting/electron transport layer (EML/ETL), and a metal cathode, as shown in Fig. 1, it is obvious that this device can be considered as a microcavity with a very weakly reflecting bottom mirror. It has been shown that weak microcavity effects can be observed in such simple bilayer OLEDs [12]. If

we consider the refractive indices of the organic materials used [13], the ITO [14] anode, and the glass substrate, the reflectance from the bottom side is just a few percent, but this is still sufficient to affect the emission pattern of an OLED and result in a dependence of the emission wavelength and intensity on the organic layer thickness and possibly the cathode choice.

Therefore, in this work we investigated the influence of the cathode choice, organic layer thickness, and the position of the emission region to the output from an OLED consisting of N,N'-diphenyl-N,N'-(3-methylphenyl)-1,1'-biphenyl-4,4'-diamine (TPD) or N,N′-di(naphthalene-1-yl)-N,N′-diphenylbenzidine (NPB) as a hole transport layer (HTL) and tris(8-hydroxyquinoline) aluminum (Alq_3) as emitting/electron transport layer (EML/ETL). The cathodes considered are the structures commonly used in OLEDs: Mg/Ag, Ca/Ag, LiF/Al, and Ag. The model fully takes into account the dispersion in all the layers in the structure. The organic layer thickness values chosen are between 30 and 250 nm, and the position of the emission region close to the metal cathode have not been considered in order to avoid unrealistic predictions since the model does not take into account exciton quenching due to defect states introduced during metal deposition. The calculations have been compared with the experimental data for ITO/NPB/Alq_3/LiF/Al and ITO/NPB/Alq_3/Ag devices. The paper is organized as follows. In the following section, the description of the model is given. In Section 3, experimental conditions are described. The results and discussion are presented in Section 4. Finally, conclusions are drawn.

2. DESCRIPTION OF THE MODEL

This paper investigates the effect of cathode metal and the position of the emission region on the spectral and luminous characteristics of the OLED. We analyzed conventional OLEDs fabricated on ITO glass substrates as microcavity devices with ITO/glass considered as a bottom mirror. Due to the small index offset between the ITO and the adjacent HTL the cavity effects are weak. Resonant

modes of the microcavity have to satisfy the condition that the phase change during one round trip is a multiple of 2π. In other words, for normal incidence, the following equation is valid:

$$\sum_i \frac{4\pi}{\lambda} d_i n_i(\lambda) - \varphi_{top}(0,\lambda) - \varphi_{bot}(0,\lambda) = 2m\pi\,, \tag{1}$$

where λ is the emission wavelength, $\varphi_{top}(\lambda)$, $\varphi_{bot}(\lambda)$ are the wavelength dependent phase changes upon reflection from top and bottom mirrors, respectively, m is an integer which defines the mode number, and the summation in is performed over all the layers inside the cavity with thicknesses d_i and refractive indices $n_i(\lambda)$. The phase shift upon reflection from the mirrors is calculated using the matrix method. The wavelength dependence of the index of refraction for aluminum (Al) and silver (Ag) was modeled using Brendel-Borman's model, with model parameters given in [15]. The refractive index of magnesium was modeled by oscillator (Lorentz-Drude) model with parameters given in [16], while optical constants of calcium films were obtained from the recent work of Ramsdale and Greenham [17]. The refractive index of Alq_3 and TPD was modeled using Cauchy equation $n(\lambda)=A+B/\lambda^2+C/\lambda^4$, where the coefficients A, B, and C were determined by fitting the data in [13]. The refractive index of NPB was determined from the spectroscopic ellipsometry measurements of an NPB film on a Si substrate. Ellipsometric measurements were taken at the incident angles of 65, 70, and 75 degrees, in the wavelength range of 300 – 1000 nm. The index of refraction of NPB was modeled using a two oscillator Lorentz model, and three incident angles were fitted simultaneously. The refractive index of ITO was modeled using the model given in [14]. As all devices investigated here are bottom emitting, the reflection from the back face of the glass substrate needs to be considered as well. The reflection coefficient was determined by applying matrix formalism with incoherent substrate correction using the modified matrix approach of

Katsidis and Siapkas [18-19]. The refractive index of glass was described using a Cauchy equation. The external emission spectrum of the OLED is given by [10-11]:

$$I_{cav}(\lambda) = \frac{\frac{1-R_{bot}}{i}\sum_{i}\left[1+R_{top}+2\sqrt{R_{top}}\cos\left(\frac{4\pi z_i}{\lambda}-\varphi_{top}\right)\right]}{1+R_{bot}R_{top}-2\sqrt{R_{bot}R_{top}}\cos\left(\frac{4\pi L}{\lambda}-\varphi_{top}-\varphi_{bot}\right)} I_{nc}(\lambda), \qquad (2)$$

where $L=\sum_j n_j d_j$ is the optical thickness of the cavity, z_i is the optical distance of the emitting dipoles to the metal mirror (cathode) with reflectivity R_{top}, R_{bot} is the reflectivity of bottom mirror (ITO/glass), $I_{nc}(\lambda)$ is the free space emission of the emitting material, and the summation over i is performed assuming that the dipoles are located within 10 to 20 nm from the HTL/emitting layer interface [10]. The actual thickness of the emitting layer depends on the exciton diffusion length, and therefore can be affected by the quality of organic layers (deposition rate, purity of materials, vacuum level, interface surface roughness), as well as the driving current and environmental factors since organic materials are very sensitive to temperature and atmosphere exposure.

3. EXPERIMENTAL DETAILS

The materials used (Alq3 from Syntech GmbH, and NPB from H. W. Sands Corp.) were purified by vacuum sublimation before fabrication. ITO substrates with nominal sheet resistance of 40 ohm/square were supplied by Varitronix Limited, Hong Kong. All the ITO substrates were cleaned before fabrication with the following cleaning procedure: the substrates were first rinsed by ethanol, acetone, toluene, then acetone, ethanol, and deionized (DI) water. After that, the substrates were cleaned in ultrasonic bath for 10 minutes in acetone, ethanol, and DI water, and dried in an oven at around 90 degree Celsius. We have performed optimal surface treatment of the cleaned ITO

according to previously reported results [20] by dipping the ITO into 12% aqueous solution of HCl for 15 minutes, followed by 15 minutes UV-ozone treatment.

Devices were fabricated by vacuum deposition. The pressure during evaporation was of the order 10^{-4} Pa. The evaporation rate was kept at 1Å/s - 2Å/s. The distance from source to film was about 23 cm to ensure uniformity of film thickness, and the substrate holder was rotating. The thickness of the films was controlled by a quartz thickness monitor. After evaporation, film thickness was verified using a Dektak 3 step profiler. The electrode consisted of 0.5 nm LiF and 100 nm Al. Eight cells were fabricated on each ITO substrate in one fabrication, and fabrications were repeated several times to verify reproducibility of the obtained results. The electroluminescence (EL) was determined using luminance-current-voltage (L-I-V) characteristics that were measured in ambient environment using a Keithley 2400 sourcemeter and Oriel MS 260I monochromator with integrating sphere and CCD detector. Photoluminescence (PL) spectra were recorded using a Perkin Elmer Instruments LS50B Luminescence Spectrometer for an excitation wavelength of 350 nm.

4. RESULTS AND DISCUSSION

As we have mentioned before, the cavity effects in structures used in this study (shown in Fig. 1) are relatively weak. The substrate used is 1 mm thick glass where the anode is a 50 nm thick ITO layer. We investigated four different metallic cathode structures, namely: LiF 0.5nm|Al 100nm, Mg 30 nm|Ag 70 nm, Ag 80 nm, and Ca 30 nm| Ag 70 nm. Figure 2 shows the calculated effect of the cavity length on the electroluminescent spectra of devices with these four different top metallic mirrors.

All four structures show similar patterns of dependence on the cavity thickness: monotonic increase in extracted EL intensity with increasing cavity thickness [solid lines in Figs. 2(a) to (d)] up

to the value corresponding to the first longitudinal mode of the cavity. Beyond the resonant thickness the intensity is decreasing (lines with markers). Structures with LiF/Al, Mg/Ag and Ag mirrors have similar optical behavior due to the strong free-electron-like behaviour of these metals. The device with Ca/Ag mirror has significantly reduced EL intensity due to the lower reflectivity of calcium in comparison to the other cathodes used. In all cases strong enhancement in extracted EL intensity was obtained for cavity lengths corresponding to the resonance of the first longitudinal mode of the cavity given by Eq. (1) notwithstanding the fact that the bottom mirror has very low reflectivity. In all calculations we assumed physical thicknesses of the HTL (TPD) and the ETL (Alq3) layers equal to 0.5 of the cavity length. Figure 3(a) shows the calculated peak EL intensity as a function of the cavity thickness. First three devices have the optimal thickness close to 140 nm, while the Ca/Ag cathode structure allows for a reduced cavity thickness. Figure 3(b) shows the magnitude of the EL peak as a function of Alq_3 layer thickness. It should be noted that our calculations deal with optical factors only. Actual EL intensity will also depend on the charge transport properties in the organic layers and the electron injection efficiency of the cathode. In this work, we mainly study the optical effects of changing the layer thickness, interface position, and the cathode material. In future work, the optical design considerations will be combined with the electronic design issues to present comprehensive guidelines for efficient OLED fabrication.

Figure 4 shows the dependence of the extracted EL spectrum on the position of the light emitting layer. For all four structures, we used the total cavity length corresponding to the first longitudinal mode (m = 1); we changed the thickness of the ETL (Alq3) to investigate the effect of the position of the light emitting layer on the EL spectrum. Thin, electrically unsuitable layers (thinner than 30 nm) have been avoided in calculations. The difference between the refractive indices of TPD and Alq3 is less than 1% in the vicinity of 530 nm (position of the EL peak of the

noncavity device). Therefore, the total physical cavity length is almost independent of the position of the TPD/Alq3 interface. This enabled us to single out and investigate the effect of the position of the emitting layer on the EL spectrum, without altering the other parameters of the optical design of the cavity. However, one has to bear in mind that changing the relative thicknesses of HTL and ETL (TPD and Alq3 respectively) electron transport will be significantly affected due to the different carrier mobility in the two layers. The mobility of electrons in Alq_3 is about two orders of magnitude lower than the hole mobility in TPD [21]. Therefore, changing the thickness of these two layers will significantly affect the balance between electrons and holes reaching the interface, and thus affect the emission intensity.

We will now have a closer look at the LiF/Al mirror device, since LiF/Al is the most commonly used cathode in OLEDs. The thickness of the Alq3 layer was changed from 30 to 110 nm. The total thickness of the cavity spacer was kept at 151 nm, corresponding to the wavelength of the $m = 1$ resonant mode of the cavity. The effect of the position of the TPD/Alq3 interface on the electroluminescence spectrum in an OLED with LiF/Al mirror is shown in Fig 4(a). Clearly the strongest EL enhancement is obtained when the emission layer is aligned with the position of the antinode of the resonant cavity [22]. Fig 5 depicts the electric field intensity in the optimally designed cavity with the HTL/ETL interface (emission layer) located at the antinode of the electric field. The phase shift on reflection from the metal mirror plays the critical role in determining the position of the antinode of the electric field. It is well known that the optical constants of metallic films depend strongly on the evaporating conditions and evaporation rate [15]. Optical constants of aluminum in particular may vary significantly due to the variable surface roughness of the film and due to the rapid volume oxidation of the aluminum film, unless the evaporation was performed in ultrahigh vacuum.

It is usually assumed that the light emission occurs from the 20 nm thick layer of Alq3 adjacent to the TPD/Alq3 interface [10]. Figure 6 shows the calculated dependence of the EL intensity and EL peak wavelength as a function of the emission region's thickness. To investigate the effect of the thickness of this region we selected two devices with interface positions (emitting region positions) located on the opposite sides of the standing wave maximum. The thickness of the emission region within the Alq3 film was varied between 5 nm and 20 nm. By reducing the thickness of the emission region of the 111 nm TPD|40 nm Alq3 structure the position of the emission region is effectively better aligned with the antinode position of the field. The other structure (76 nm TPD/75 nm Alq3) is effectively misaligned by the reduction on the emission region thickness. Therefore, to maximize the emitted power, the antinode of the optical field should be aligned with the middle of the emission region. This makes the thickness of the Alq3 layer in the optimally designed device dependent on the thickness of the light emission region. As pointed out before, emission region thickness is determined by the exciton diffusion length. The exciton diffusion length can be affected by the experimental parameters, such as the purity of material used, vacuum level during deposition, deposition rate etc., as well as experimental conditions during measurement, such as bias, temperature, and measurement environment (with or without encapsulation, in atmosphere or in inert gas). Since some of the experimental factors may be difficult to control in a reliable and reproducible manner, it is difficult to ensure that all the fabricated devices would have the same emission region width. However, it is possible to artificially confine the excitons by insertion of an additional wide band gap organic layer such as bathocuproine, which is typically used in organic light emitting diodes and organic solar cells as a hole blocking or exciton blocking layer [23-24]. In such a manner, the width of the emission region can be made sufficiently narrow and very reproducible. The width of the emission region can also be reduced by doping (with low dopant concentrations) [25].

Figure 7 shows the refractive indices of the organic materials considered (Alq_3 as emission layer and TPD or NPB as hole transport layer). The small difference between our result and the Cauchy model for the refractive index of Alq in Ref. [13] is likely due to different source and purity of the organic materials, and different procedures for extraction of the experimental data. While these materials have similar refractive indices in the spectral region of interest, and thus their optical properties will not affect the device performance, there are other factors which need to be considered in order to fabricate efficient OLED devices. As already mentioned, there are significant differences in the carrier mobility [21]. In addition, the choice of the hole transport layer affects the hole injection efficiency from the ITO electrode into the organic material [26]. Also, higher glass transition temperature of NPB (90-100°C, compared to 60-70°C for TPD [27]) results in improved stability. Higher luminous efficiency for the same device structure can be obtained when NPB is used instead of a TPD layer [28]. Thus, although calculation results are valid for devices using both conventional hole transport layers due to their similar optical properties, for the comparison with the experimental data, devices with NPB as a HTL were fabricated to ensure high brightness and sufficient lifetime for detailed characterizations such as angular dependence of the emission.

Figure 8 compares the calculated and experimental EL spectra for two devices fabricated with LiF/Al mirror and with two different thicknesses of the Alq3 layer: 250 nm and 167 nm. The spectra reveal shifts in peak positions similar to those predicted by the optical model. We have chosen to model the EL spectra since in the case of PL the emission region is not as clearly determined as in the case of EL. For EL, excitons are created at the NPB/Alq interface and the emission region width is determined by the exciton diffusion length. For PL, the excitons can be generated throughout the Alq layer, but we cannot analytically account for the quenching near the interface with the metal cathode. Thus, a comparison between EL and the calculated spectra is more realistic. Excellent

agreement can be observed between the calculated and the experimental peak positions. The experimental spectra, however, exhibit larger broadening than the calculated spectra. This is likely due to some complex experimental factors, such as enhanced Joule heating around pinhole or defect areas, emissive layer degradation due to formation of unstable Alq_3 cation species or reaction with oxygen and water in the atmosphere etc., which may affect the obtained results. In order to obtain better agreement with the experimental data, it would be necessary to fully take into account the charge injection, charge transport, and exciton diffusion in modeling the emitted spectra. Work is in progress to develop a comprehensive model taking into account both electronic and optical properties of all the layers in the device.

5. CONCLUSION

In conclusion, we have presented calculations of the emitted radiation from organic OLEDs as a function of the choice of cathode, the thickness of organic layers, and the position of the hole transport layer/Alq_3 interface. Four cathode structures have been considered: Mg/Ag, Ca/Ag, LiF/Al, and Ag. For the hole transport layer, N,N'-diphenyl-N,N'-(3-methylphenyl)-1,1'-biphenyl-4,4'-diamine (TPD) and N,N′-di(naphthalene-1-yl)-N,N′-diphenylbenzidine (NPB) were used, while tris(8-hydroxyquinoline) aluminum (Alq_3) was the emitting layer. It was found that the emission spectrum is strongly dependent on the layer thickness, interface position, as well as thickness of the emission region. For the optimal efficiency, the emission region should be narrow and its centre aligned with the antinode of the electric field in the resonant cavity. Since the emission region width depends on the exciton diffusion length, in order to confine the excitons to a narrow region insertion of an additional exciton blocking layer or doping of the emitting layer may be advisable. Our simulation results show good agreement with the experiment. The objective of our work was to

analyze an OLED structure from an optical point of view, and the electronic considerations (electron injection and charge transport) were not taken into account. In order to obtain better agreement with electroluminescence experimental data, it will be necessary to integrate the electrical and optical models. Inclusion of electron injection efficiency for different cathodes and the charge transport in the organic layers will also ensure better prediction of electroluminescence intensity for devices with different cathodes.

ACKNOWLEDGEMENTS

This work has been partially supported by the RGC earmarked grant of Hong Kong (Project HKU 7056/02E) and the University of Hong Kong University Research Committee seed funding grant.

REFERENCES

1. W. Brütting, S. Berleb, and A. G. Muckl, “Device physics of organic light-emitting diodes based on molecular materials”, Organic Electronics **2**, pp. 1-36, March 2001.

2. L. S. Hung and C. H. Chen, “Recent progress of molecular organic electroluminescent materials and devices”, Mat. Sci. Eng. R **39**, pp. 143-202, Dec. 2002.

3. B. K. Crone, P. S. Davids, I. H. Campbell, and D. L. Smith, “Device model investigation of bilayer organic light emitting diodes”, J. Appl. Phys. **87**, pp. 1974-1982, Feb. 2000.

4. E. Tutiš, D. Berner, and L. Zuppiroli, Internal electric field and charge distribution in multilayer organic light-emitting diodes, J. Appl. Phys. **93**, pp. 4594-4602, Apr. 2003.

5. J.-S. Kim, P. K. H. Ho, N. C. Greenham, and R. H. Friend, Electroluminescence emission pattern of organic light-emitting diodes:Implications for device efficiency calculations, J. Appl. Phys. **88**, pp. 1073-1081, July 2000.

6. M.-H. Lu and J. C. Sturm, Optimization of external coupling and light emission in organic light-emitting devices: modeling and experiment, J. Appl. Phys. **91**, pp. 595-604, Jan. 2000.

7. S. K. So, W. K. Choi, L. M. Leung, and K. Neyts, Interference effects in bilayer organic light-emitting diodes, Appl. Phys. Lett. **74**, pp. 1939-1941, Apr. 1999.

8. H. Riel, S. Karg, T. Beierlein, W. Rieβ, and K. Neyts, Tuning the emission characteristics of top-emitting organic light-emitting devices by means of a dielectric capping layer: An experimental and theoretical study, J. Appl. Phys. **94**, pp. 5290-5296, Jan. 2003.

9. H. Riel, S. Karg, T. Beierlein, B. Ruhstaller, and W. Rieβ, Phosphorescent top-emitting organic light-emitting devices with improved light outcoupling, Appl. Phys. Lett. **82**, pp. 466-468, Jan. 2003.

10. A. Dodabalapur, L. J. Rothberg, R. H. Jordan, T. M. Miller, R. E. Slusher, and J. M. Phillips, Physics and applications of organic microcavity light emitting diodes, J. Appl. Phys. **80**, pp. 6954-6964, Dec. 1996.

11. T. Shiga, H. Fujikawa, and Y. Taga, Design of multiwavelength resonant cavities for white organic light emitting diodes, J. Appl. Phys. **93**, pp. 19-22, Jan. 2003.

12. V. Bulović, V. B. Khalfin, G. Gu, P. Burrows, D. Z. Garbuzov, and S. R. Forrest, Weak microcavity effects in organic light-emitting devices, Phys. Rev. B **58**, pp. 3730-3740, Aug. 1998.

13. F. G. Celii, T. B. Harton, and D. F. Philips, "Characterization of organic thin films for OLEDs using spectroscopic ellipsometry", J. Electron. Mater. **26**. pp. 366-371, April 1997.

14. S. Laux, N. Kaiser, A. Zöller, R. Götzelmann, H. Lauth, and H. Bernitzki, "Room-temperature deposition of indium tin oxide thin films with plasma ion-assisted evaporation", Thin Solid Films **335**, pp. 1-5, Nov. 1998.

15. A. D. Rakić A. B. Djurišić, J.M. Elazar and M. L. Majewski, "Optical properties of metallic films for vertical-cavity optoelectronic devices", Appl. Opt. **37**, pp. 5271-5283, Aug. 1998.

16. R. Machorro, J. M. Siqueiros, and S. Wang,"Optical properties of Mg, from UV to IR, using ellipsometry and reflectometry", Thin Solid Films 269, pp. 1-5, Nov. 1995.

17. C. M. Ramsdale and N. C. Greenham, "The optical constants of emitter and electrode materials in polymer light-emitting diodes". J. Phys. D: Appl. Phys. **36**, pp. L29-L34, Feb. 2003.

18. C. C. Katsidis and D. I. Siapkas, "General transfer-matrix method for optical multilayer systems with coherent, partially coherent, and incoherent interference", Appl. Opt. **41**, pp. 3978-3987, July 2002.

19. C. L. Mitsas and D. I. Siapkas, “Generalized matrix-method for analysis of coherent and incoherent reflectance and transmittance of multilayer structures with rough surfaces, interfaces, and finite substrates”, Appl. Opt. **34**, pp. 1678-1683, Apr. 1995.

20. C. N. Li, A. B. Djurišić, C. Y. Kwong, P.T. Lai, W. K. Chan, and S. Y. Liu, “Indium tin oxide surface treatments for improvement of organic light emitting diode performance”, accepted for publication in Appl. Phys. A, 2003.

21. S. Naka, H. Okada, H. Onnagawa, Y. Yamaguchi, and T. Tsutsui, “Carrier transport properties of organic materials for EL device operation”, Synth. Met. **111-112**, pp. 331-333, June 2000.

22. Y. Yamamoto, S. Machida, K. Igeta and G. Bjork, “Controlled Spontaneous Emission in Microcavity Semiconductor Lasers” in Y. Yamamoto Ed. “Coherence, Amplification and Quantum Effects in Semiconductor Lasers”, J. Wiley and Sons, Inc. New York, 1991.

23. F. Li, M. Zhang, J. Feng, G. Cheng, Z. Wu, Y. Ma, S. Liu, J. Sheng, and S. T. Lee, “red electrophosphorescence devices based on rhenium complexes”, Appl. Phys. Lett. **83**, pp. 365-367, July 2003.

24. P. Peumans and S. R. Forrest, Very-high-efficiency double-heterostructure copper phthalocyanine/C_{60} photovoltaic cells, Appl. Phys. Lett. **79**, pp. 126-128, July 2001.

25. J. Kalinowski, L. C. Picciolo, H. Murata, and Z. H. Kafafi, “Effect of emitter disorder on the recombination zone and the quantum yield of organic electroluminescent devices”, J. Appl. Phys. **89**, pp. 1866-1874, Feb. 2001.

26. C. Giebeler, H. Antoniadis, D. D. C. Bradley, and Y. Shirota, “Influence of the hole transport layer on the performance of organic light-emitting diodes”, J. Appl. Phys. **85**, pp. 608-615, Jan. 1999.

27. M. Carrard, S. Conto-Gonclaves, L. Si-Ahmed, D. Ades, and A. Siove, “Improved stability of interfaces in organic light emitting diodes with high T_g materials and self-assembled monolayers”, Thin Solid Films 352, pp. 189-194, Sep. 1999.

28. C. N. Li, A. B. Djurišić, C. Y. Kwong, P.T. Lai, W. K. Chan and S. Y. Liu, “Indium tin oxide surface treatments for improvement of organic light emitting diode performance”, Applied Physics A, in press, 2004.

Figures

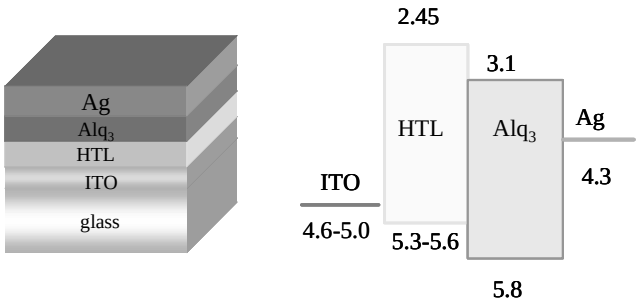

Figure 2

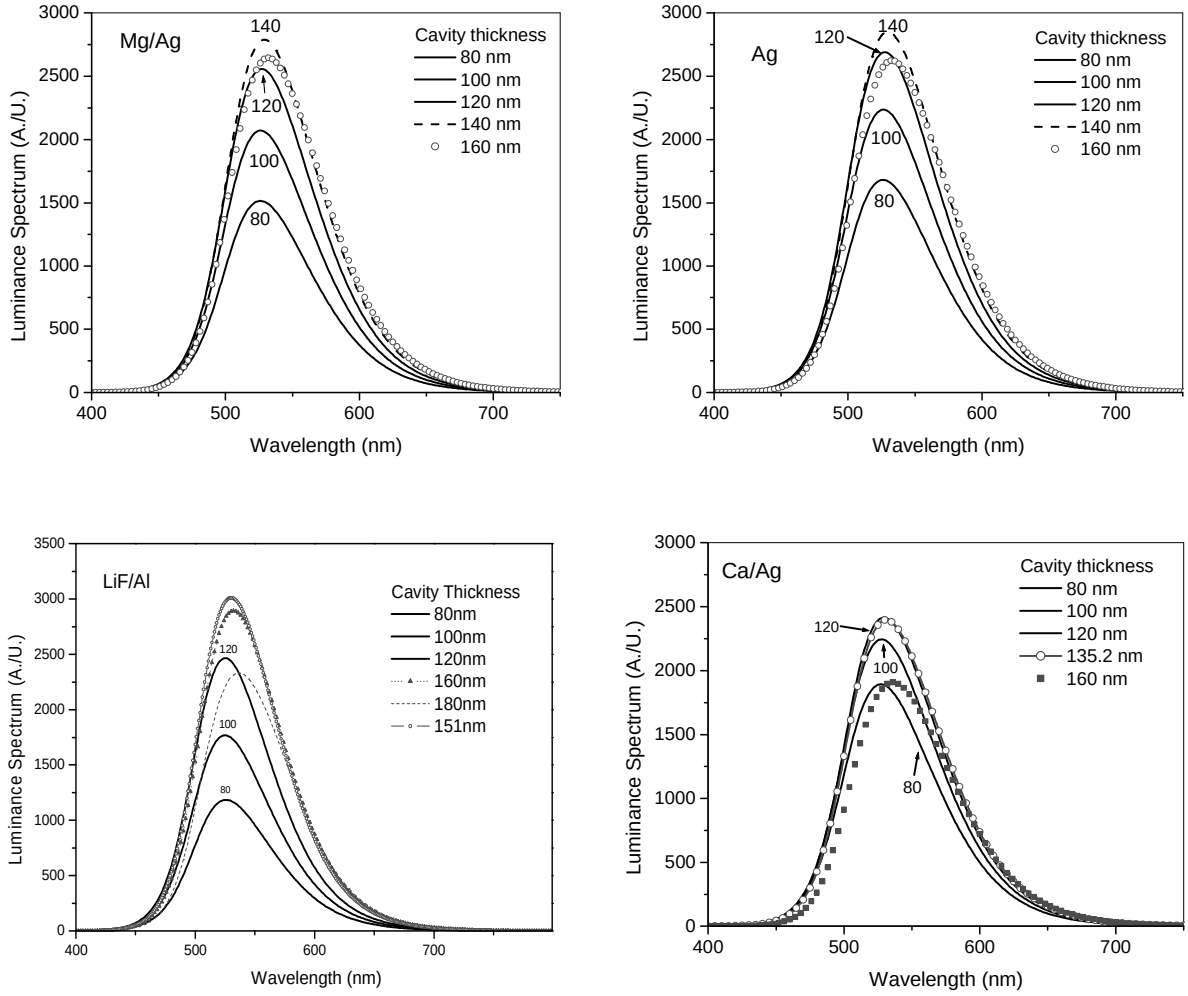
Mg/Ag
Cavity thickness
80 nm
100 nm
120 nm
140 nm
160 nm
140
120
100
80
Luminance Spectrum (A./U.)
Wavelength (nm)
Ag
Cavity thickness
80 nm
100 nm
120 nm
140 nm
160 nm
120
140
100
80
Luminance Spectrum (A./U.)
Wavelength (nm)
LiF/Al
Cavity Thickness
80nm
100nm
120nm
160nm
180nm
151nm
120
100
80
Luminance Spectrum (A./U.)
Wavelength (nm)
Ca/Ag
Cavity thickness
80 nm
100 nm
120 nm
135.2 nm
160 nm
120
100
80
Luminance Spectrum (A./U.)
Wavelength (nm)

Figure 2

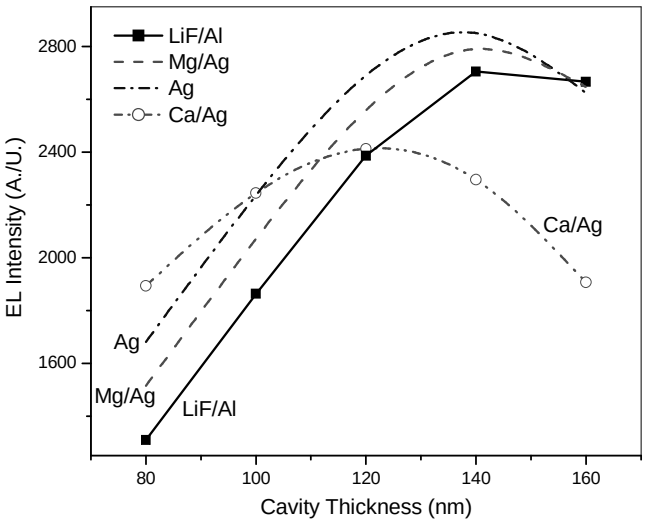

Figures 3(a)

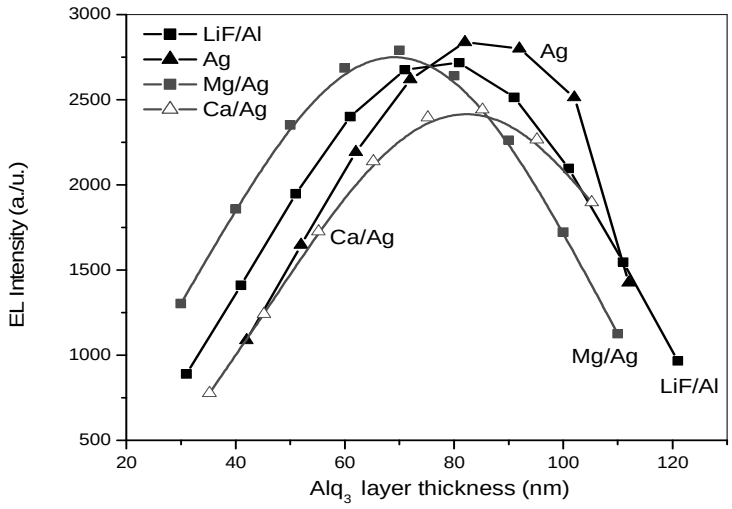

Figure 3(b)

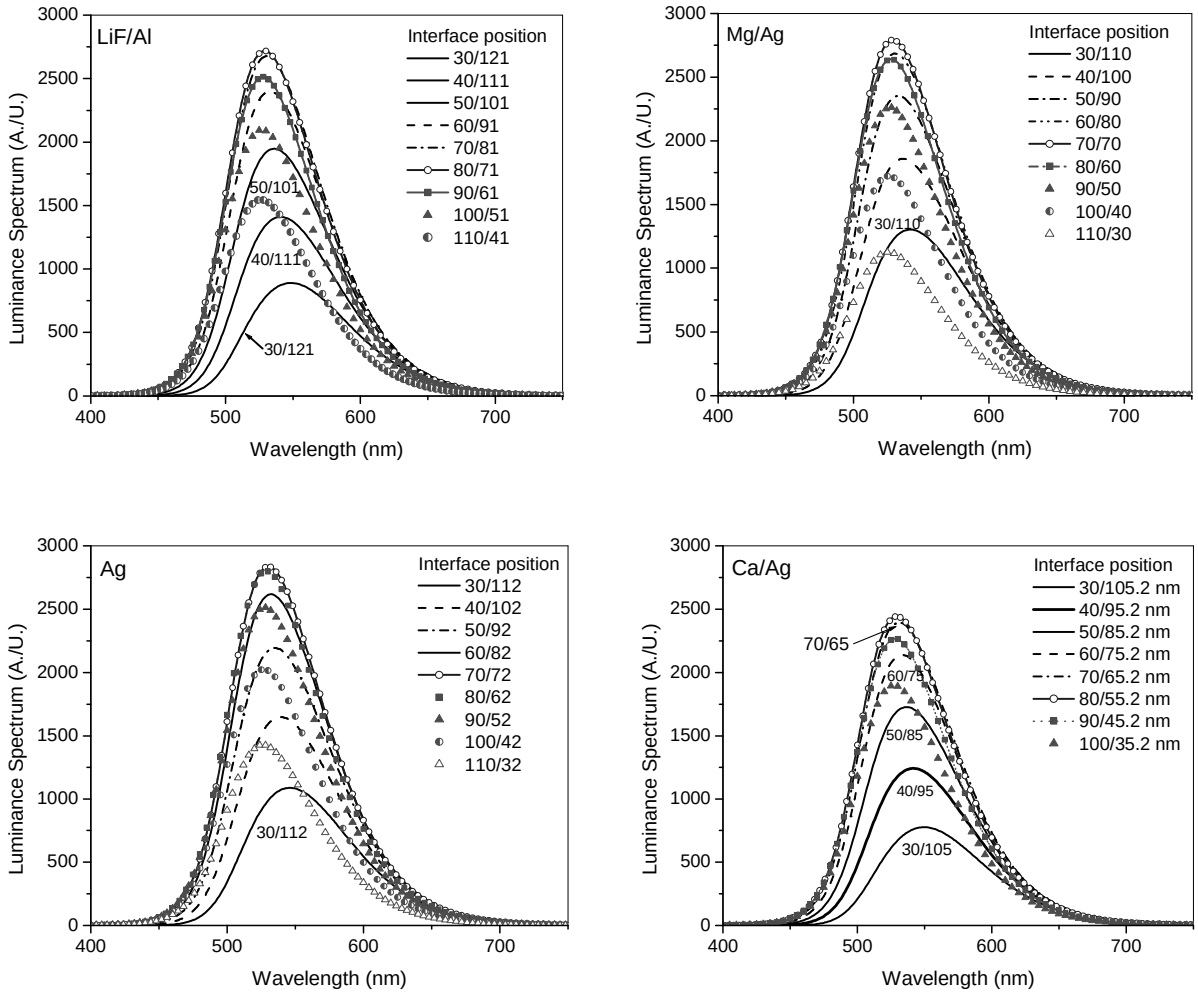
LiF/Al
Interface position
30/121
40/111
50/101
60/91
70/81
80/71
90/61
100/51
110/41
50/101
40/111
30/121
Luminance Spectrum (A./U.)
Wavelength (nm)
Mg/Ag
Interface position
30/110
40/100
50/90
60/80
70/70
80/60
90/50
100/40
110/30
30/110
Ag
Interface position
30/112
40/102
50/92
60/82
70/72
80/62
90/52
100/42
110/32
30/112
Ca/Ag
Interface position
30/105.2 nm
40/95.2 nm
50/85.2 nm
60/75.2 nm
70/65.2 nm
80/55.2 nm
90/45.2 nm
100/35.2 nm
70/65
60/75
50/85
40/95
30/105

Figure 4

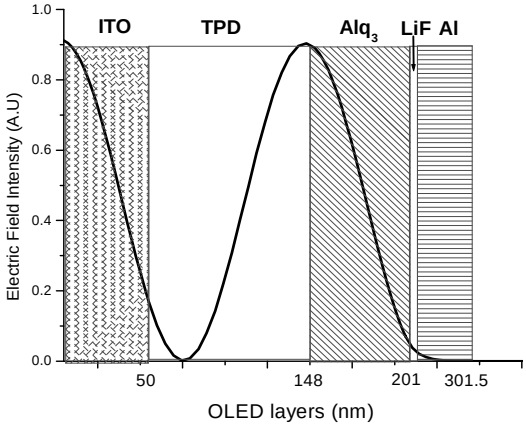
ITO
TPD
Alq3
LiF
Al
Electric Field Intensity (A.U)
1.0
0.8
0.6
0.4
0.2
0.0
50
148
201
301.5
OLED layers (nm)

Figure 5

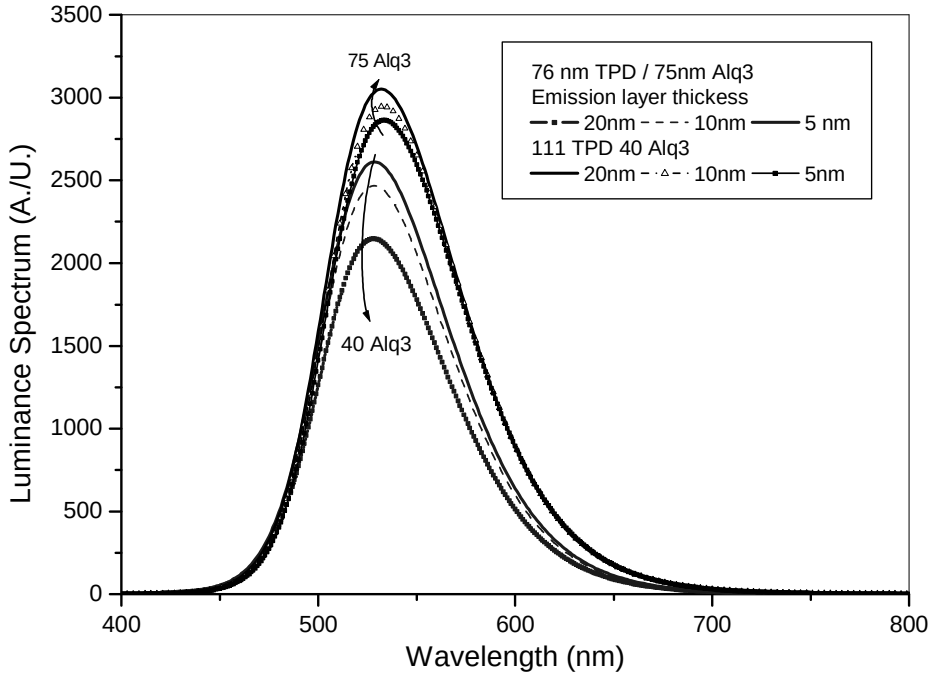
Luminance Spectrum (A./U.)
Wavelength (nm)
75 Alq3
40 Alq3
76 nm TPD / 75nm Alq3
Emission layer thickess
20nm
10nm
5 nm
111 TPD 40 Alq3
20nm
10nm
5nm

Figure 6

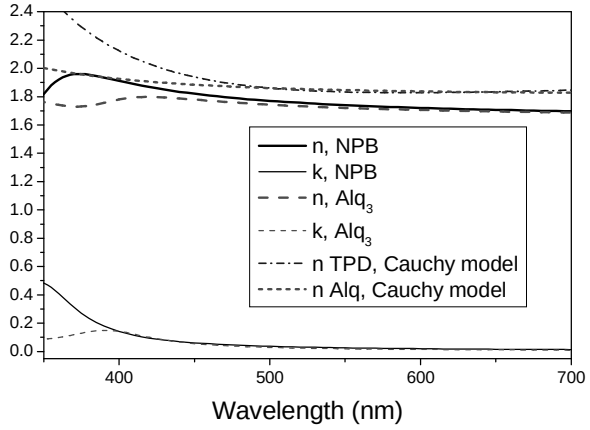
2.4
2.2
2.0
1.8
1.6
1.4
1.2
1.0
0.8
0.6
0.4
0.2
0.0
400
500
600
700
Wavelength (nm)
n, NPB
k, NPB
n, Alq3
k, Alq3
n TPD, Cauchy model
n Alq, Cauchy model

Figure 7

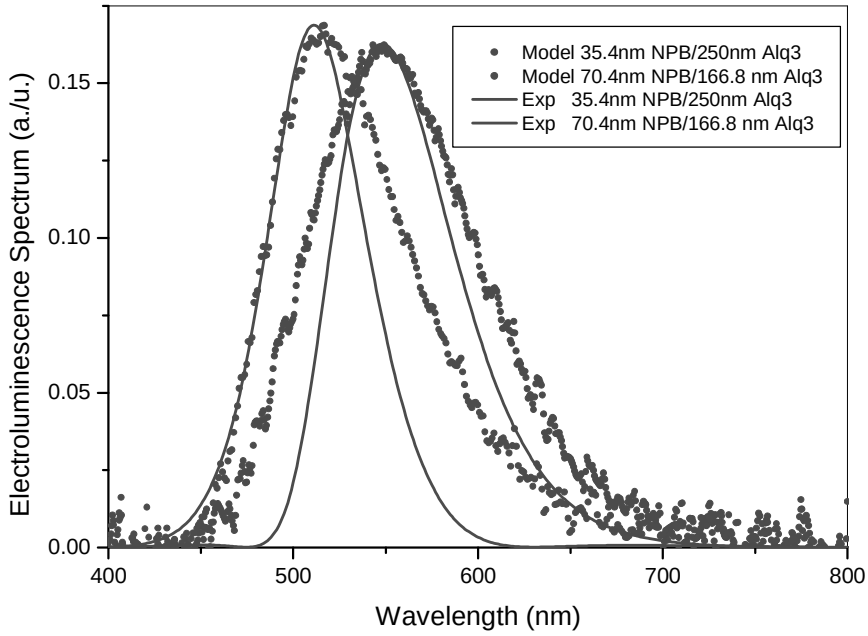
Model 35.4nm NPB/250nm Alq3
Model 70.4nm NPB/166.8 nm Alq3
Exp 35.4nm NPB/250nm Alq3
Exp 70.4nm NPB/166.8 nm Alq3
Electroluminescence Spectrum (a./u.)
0.00
0.05
0.10
0.15
400
500
600
700
800
Wavelength (nm)

Figure 8